ACS APPLIED MATERIALS & INTERFACES

Research Article

www.acsami.org

Competitive Assembly To Increase the Performance of the DNA/Carbon-Nanomaterial-Based Sensing Platform

Qiao Tang, Qier Zhang, Ying Jiang, Jishan Li,* Jing Zheng, Yinhui Li, Ronghua Yang,* and Weihong Tan

State Key Laboratory of Chemo/Biosensing and Chemometrics, College of Chemistry and Chemical Engineering, Hunan University, Changsha 410082, China

Supporting Information

ABSTRACT: Increasing the rate of target binding on the surface and enhancing the fluorescence signal restoration efficiency are critical to the desirable biomedical application of carbon nanomaterials, for example, single-walled carbon nanotubes (SWNTs). We describe here a strategy to increase the target binding rate and enhance the fluorescence signal restoration efficiency on the DNA-functionalized SWNT surface using a short complementary DNA (scDNA) strand. The scDNA causes up to a 2.5-fold increase in association rate and 4-fold increase in fluorescence signal restoration by its competitive assembly on the nanostructure's surface and inducing a conformational change that extends the DNA away from the surface, making it more available to bind target nucleic acids. The scDNA-induced enhancement of binding kinetics and fluorescence signal restoration efficiency is a general phenomenon that occurred with all sequences and surfaces investigated. Through this competitive assembly strategy of scDNA, performance improvement of the carbon-nanomaterial-based biosensing platform for both in vitro detection and live cell imaging can be reached.

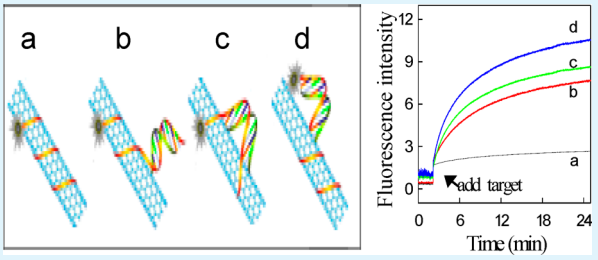

KEYWORDS: *carbon nanomaterials, competitive assembly, interface, short complementary DNA, biosensors*

1. INTRODUCTION

A unique ability for DNA adsorption[1−3] as well as their superquenching capacity with a wide energy transfer range[4−8] has shown single-walled carbon nanotubes (SWNTs) to be a robust artificial nanomaterial in bionanotechnology, with applications in DNA analysis,[9−14] protein assays,[15−17] cellular imaging, etc.[18] However, this DNA/SWNT-nanocomplex-based biosensing platform has serious limitations such as poor fluorescence restoration and slow response kinetics due to the strong affinity of the flat carbon nanostructures for ssDNA via π-stacking and hydrophobic interactions.[19,20] Therefore, there is a major need to improve the speed and efficiency of this nanocomplex-based biosensing platform for medical diagnostics, cellular imaging, and molecular biology. Recently, Mirkin and co-workers have successfully used a short internal complementary DNA (sicDNA) strand to increase the rate of target hybridization on DNA covalently functionalized gold surfaces.[21] However, improving the performance of target hybridization on the carbon nanostructure surface appears to be rare. Therefore, we present herein a DNA-competitive-assembly-based strategy by using short complementary DNA (scDNA) to improve the performance of the DNA/carbon-nanomaterial-based sensing platforms.

As we all know, single-stranded DNA (ssDNA) can wrap around an SWNT by means of π-stacking interactions between the nucleotide bases and the SWNT sidewall to form a stable complex, and double-stranded DNA (dsDNA) can also interact with an SWNT, although its affinity is much weaker than that of ssDNA.[19] Therefore, the strong affinity of SWNTs for ssDNA and the weak ability of SWNTs to distinguish ssDNA and dsDNA resulted in slow response kinetics and poor fluorescence restoration in DNA/SWNT-nanocomplex-based biosensing systems. Therefore, considering the stronger adsorbing affinity of SWNTs for ssDNA than for dsDNA or other target−DNA complexes, we hope that the use of an scDNA which can hybridize with part of the fluorophore-labeled DNA probe sequence can improve the performance of DNA/SWNT-nanocomplex-based biosensing platforms via scDNA competitive assembly. The introduction of an scDNA has two expected functions: (1) to increase the response kinetics via weakening of the adsorption affinity of DNA sequences on the SWNT surface and moving some segments of the DNA probe sequence away from the surface for more availability to the incoming target due to the structural change and the formed dsDNA domain; (2) to enhance fluorescence restoration via competitive assembly of the released scDNA on the SWNT surface after target association and assembly inhibit dsDNA or DNA−target complexes with relatively weak affinity on the SWNT surface.

Received: April 18, 2014
Accepted: July 23, 2014
Published: July 23, 2014

dx.doi.org/10.1021/am502311b | ACS Appl. Mater. Interfaces 2014, 6, 13470−13477

Table 1. Oligonucleotide Sequences Used in This Work

type	sequence (5′ to 3′)
P1	TCAGTGGGGTTGGACGGGATGGTGCCTGA
P2	Cy5-TCAGTGGGGTTGGACGGGATGGTGCCTGA-FAM
P3	TCAGTGGGGTTGGACGGGATGGTGCCTGA-FAM
T1	TCAGGCACCATCCCGTCCAACCCCACTGA
stcDNA-1	CAACCCCACTGA
stcDNA-3	CCCACTGA
stcDNA-4	ACCCCACTGA
stcDNA-5	GTCCAACCCCACTGA
stcDNA-6	TCCCGTCCAACCCCACTGA
smcDNA	CATCCCGTCCAA
stcDNA-2	TCAGGCACCATC
stcDNA-2-FAM	TCAGGCACCATC -FAM
P4	TCAACATCAGTCTGATAAGCTA-FAM
scDNA-miR21	TGATGTTGA

Scheme 1. Schematic Illustration of Fluorescent Detection of Target DNA or Protein Based on the DNA/SWNT Sensing Ensemble in the Presence of scDNA

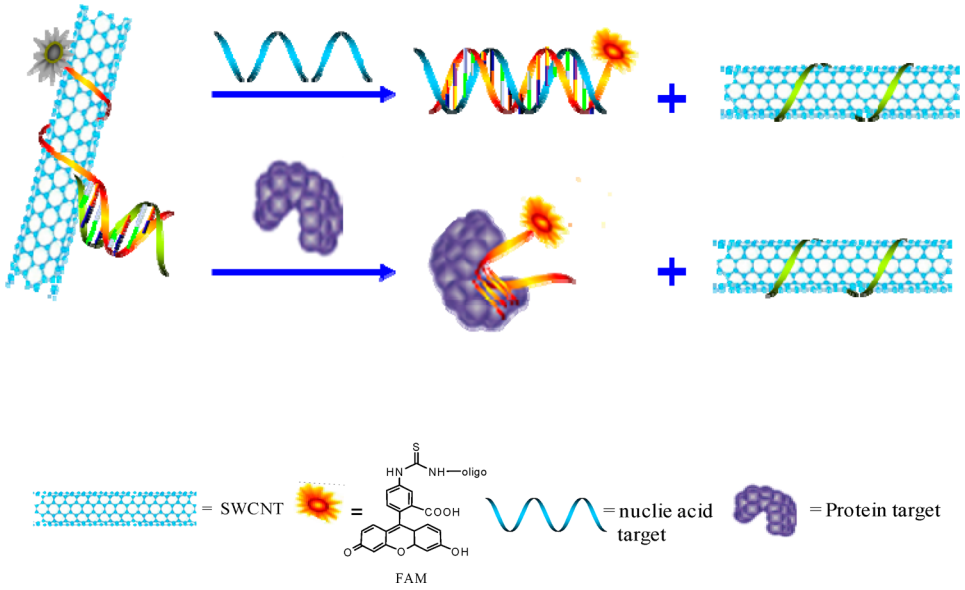

2. EXPERIMENTAL SECTION

2.1. Chemicals and Apparatus. All oligonucleotides (Table 1) were synthesized and purified by HPLC from TaKaRa Biotechnology Co., Ltd. (Dalian, China). The DNA concentration was identified according to UV absorption at 260 nm. Thrombin was purchased from Sigma-Aldrich Chemical Co. (United States). To ensure CNTs were soluble in water to control the quantitative analysis, carboxyl-functionalized SWNTs, purchased from Carbon Nanotechnologies, Inc., Houston, TX, were used. MCF-7 cells were obtained from the cell bank of the Central Laboratory at Xiangya Hospital (Changsha, China). All other chemicals (analytical reagent, AR, grade) were commercially available and used without further purification. Solutions were prepared using deionized water (18.3 MΩ·cm) produced from a Millpore water purification system, and all work solutions were prepared with 0.1 M Tris−HCl buffer solution (pH 7.4, 50 mM KCl, 10.0 mM $MgCl_2$).

The fluorescence spectra were measured using a PTI QM4 fluorescence system with a temperature control accessory (Photo Technology International, Birmingham, NJ). Both the excitation and emission slit widths were set to 5.0 nm. FAM was excited at λ_{ex} = 480 nm, and its fluorescence emission was followed at λ_{em} = 520 nm. Cy5 was excited at λ_{ex} = 633 nm, and its fluorescence emission was followed at λ_{em} = 665 nm. The pH was measured with a model 868 pH meter (Orion). The hydrodynamic radius of DNA/SWNTs was measured by dynamic light scattering (DLS) (Zetasizer Nano ZS, Malvern). For cell imaging, scanning confocal microscopy (Olympus FluoView 500) was used.

2.2. Preparation of DNA/SWNT Conjugates. A 500 nM concentration of fluorescent oligonucleotide probes with/without 500 nM scDNA in Tris−HCl buffer were first incubated for 2 h at room temperature. Then carboxyl-functionalized SWNTs were sonicated in doubly deionized water for 5 h to give a homogeneous black solution. After these pretreatments, enough SWNTs were introduced into 500 μL of the prepared DNA probe solution, and the mixture was incubated for another 2 h at room temperature. Then a centrifugation step was carried out at 3000 rpm to get rid of the SWNTs without DNA coating. The obtained supernatant (DNA/SWNTs) was stored in a refrigerator at 4 °C before further use.

2.3. Hybridization Kinetic Measurements. Hybridization rates between DNA/SWNT conjugates and their perfectly complementary DNA target were determined using fluorescence measurements recorded on a PTI QM4 fluorescence system. Complementary target DNA (T1; 50 nM) was added to 10-fold-diluted P3/SWNT or P3-scDNA/SWNT conjugates in Tris−HCl buffer (the concentration of fluorescent probe P3 was ca. 50 nM), and the change in fluorescence emission intensity at 520 nm (excitation 480 nm) over time was measured in 1 s increments. k_{obsd} for each hybridizing curve was

dx.doi.org/10.1021/am502311b | ACS Appl. Mater. Interfaces 2014, 6, 13470−13477

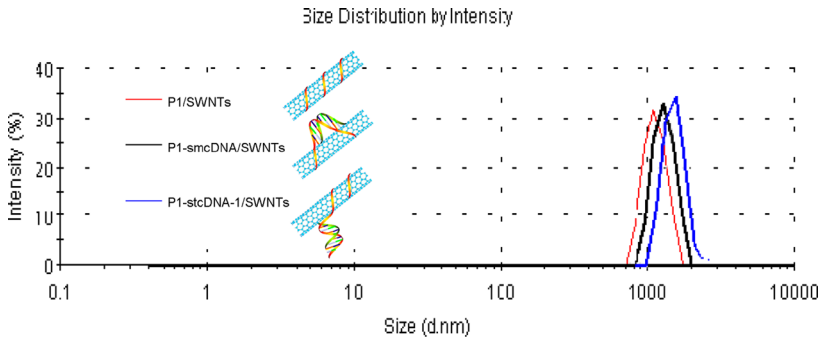

Figure 1. Size distribution of the DNA/SWNT conjugates in the presence of scDNA determined by DLS.

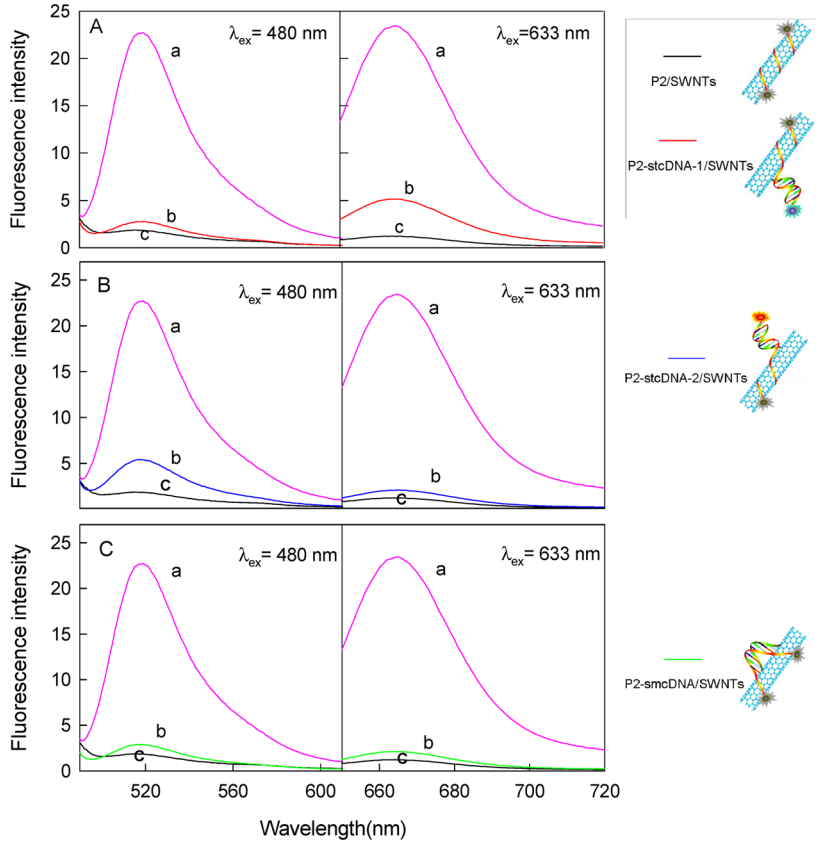

Figure 2. Fluorescence emission spectra of the DNA/SWNT conjugates in the presence of different scDNAs: (A) P2-stcDNA-1/SWNTs; (B) P2-stcDNA-2/SWNTs; (C) P2-smcDNA/SWNTs. For curve a, the concentration of P2 was 50 nM. For curve b, scDNA was introduced. Curve c is for P2/SWNTs. FAM was excited at λ_{ex} = 480 nm, and its fluorescence emission was in the range from 500 to 600 nm. Cy5 was excited at λ_{ex} = 633 nm, and its fluorescence emission was in the range from 650 to 720 nm. Both excitation and emission slits were 5 nm.

determined by fitting the data to a simple association kinetic equation ([target bound] = [target bound]$_{max}e^{k*t}$).[21]

2.4. In Vitro Detection of DNA and Protein. A 500 μL volume of 10-fold-diluted P3/SWNT or P3-stcDNA-1/SWNT conjugates (the concentration of fluorescent probe P3 was ca. 50 nM) in Tris−HCl buffer was incubated with T1 or thrombin for 30 min at 37 °C. After reaction, the resulting solution was subjected to fluorescence measurements. The fluorescence spectra were recorded at room temperature in a quartz cuvette on a PTI QM4 fluorescence system. The excitation wavelength was 480 nm, and the emission wavelengths were in the range from 500 to 600 nm with both excitation and emission slits of 5 nm. For the calibration curves, the change in fluorescence emission intensity at 520 nm was adopted.

2.5. Live Cell Imaging. MCF-7 cells were cultured in Leibovitz's L-15 medium with 2 mM L-glutamine supplemented with 10% fetal bovine serum (all reagents from Invitrogen). Cells were plated into chambered coverslides 1 day before the experiments so that cells would be about 90% confluent during the experiments. The proposed P4-stcDNA-miR21/SWNT conjugates were added to each well and incubated for 12 h at 37 °C under a CO_2 air atmosphere. After incubation, the cell medium was decanted from the well, and the cells were washed thoroughly prior to cellular imaging. Three-dimensional images were taken per micrometer by scanning the samples across a defined section along the *z*-axis.

3. RESULTS AND DISCUSSION

3.1. Investigations of the DNA/SWNT Conjugate's Structure and the Interaction Mechanism. The strategy is illustrated in Scheme 1 through two types of fluorophore-labeled DNA probes, a nucleic acid hybridization probe and an aptamer probe. To provide direct evidence for the reaction

process, a gel electrophoresis experiment was carried out (Figure S1, Supporting Information). The results show that there is no significant DNA probe band (P3) on the gel image for the supernatant of stcDNA-1-P3-wrapped SWNTs (lane 5), while for the supernatant of stcDNA-1-P3/SWNTs with addition of DNA (lane 4) or protein (lane 6) target, there is a clear DNA probe band on the gel image, indicating that the formed DNA duplex or DNA (aptamer)−protein complex fell off the SWNT surface and stayed in the supernatant after centrifugation.

The improved performance of DNA/SWNT-nanocomplex-based biosensing platforms might result from the following two distinct origins: First is the alteration of the DNA structure resulting from the formation of the dsDNA domain, thereby decreasing the adsorption affinity of the DNA probe on the SWNT surface and making it more available to the incoming target. Second is the competitive assembly of the released scDNA on the SWNT surface, thereby inhibiting the assembly of dsDNA or DNA−target complexes on the SWNs surface. Therefore, before exploration of the effect of scDNA on the performance improvement of this biosensing platform, the effect of scDNA on the interaction between the DNA probe and SWNTs and the effect of the competitive assembly ability of scDNA on the SWNT surface should be investigated carefully.

Usually, the formed DNA duplex is not stable when the base number is less than 8 bases, and a suitable sequence length is necessary for the adsorption of ssDNA on the SWNT surface, so the sequence length of scDNA was first optimized. It can be seen from Figure S2 (Supporting Information) that the fluorescence restoration efficiency with increasing scDNA length is first increased and then decreased. This result shows that if the scDNA sequence is short, the fluorescence restoration efficiency will be lower, which might result from the unsatisfactory competitive assembly ability of the scDNA on the SWNT surface and the strong adsorption affinity between the single-stranded DNA probe and SWNTs. However, if the scDNA sequence is too long, the probe system will still give lower fluorescence restoration efficiency. The reason might be that the fluorescence molecule will be moved away from the SWNT surface due to the formation of a long double-stranded structure, thus resulting in higher background fluorescence. To guarantee higher fluorescence restoration efficiency, the 12-base scDNA sequence was chosen for use in the platform investigation.

To determine whether scDNA has an effect on the structure of the DNA/SWNTs, DLS was used to measure the hydrodynamic radii of the nanocomplexes. In the presence of scDNA, located at either the terminus domain or the middle domain of P1, a slight increase of the radius can be observed (Figure 1), indicating that the introduction of scDNA resulted in a structural change of the DNA/SWNT nanocomplexes and moved the formed dsDNA domains away from the SWNT surface. Although the DLS experiment provides information about the general DNA/SWNT structure, the specific location of scDNA in the fluorescent-dye-labeled probe appears to be particularly important for an increase of the ratio of the signal to the background. To directly investigate the effect of scDNA on the interaction between the DNA probe and SWNT, a DNA sequence (P2) adsorbed onto the SWNT surface was labeled on its two distal ends with the fluorophores FAM and cy5, respectively, and the nanocomplex-associated fluorescence was measured before and after addition of the scDNA strands (Figure 2). One can see from Figure 2 that the fluorescence intensity of FAM increased significantly when scDNA (stcDNA-2) was hybridized with the FAM-labeled distal region, while there was no obvious change in the fluorescence intensity of cy5. In contrast to this, the fluorescence intensity of cy5 increased significantly while there was no obvious change for FAM when scDNA (stcDNA-1) was hybridized with the cy5-labeled distal region. When scDNA (smcDNA) was hybridized with the middle domain of the DNA probe, no obvious fluorescence change was observed for both FAM and cy5. These results, combined with the observed change in hydration radius of the nanocomplexes, suggest that the introduction of scDNA can move a certain region of the DNA probe away from the SWNT surface, which will decrease the adsorption affinity of the whole DNA probe sequence for SWNTs and at the same time make it more available to incoming targets.

The competitive assembly of the displaced scDNA on the SWNT surface is another major factor for the performance improvement of the DNA/SWNT-nanocomplex-based biosensing system. To determine whether the scDNA is still located on the SWNT surface after target binding, an scDNA was labeled on the distal end with the fluorophore FAM (stcDNA-2-FAM), and the nanocomplex (P1- stcDNA-2-FAM/SWNTs)-associated fluorescence was measured before and after the addition of DNA (T1) or protein targets (thrombin). However, no increase in FAM's fluorescence intensity, even after further fluorescence quenching, was observed for both DNA and protein targets (Figure 3). A gel electrophoresis measurement corresponding to Figure 3 was carried out to further verify the observed phenomenon (Figure S3, Supporting Information). The results show that there is no significant scDNA band (stcDNA-2-FAM) on the gel image for all the supernatants of P1-stcDNA-2-FAM/SWNTs (lane 3 of Figure S3A), P1-stcDNA-2-FAM/SWNTs + T1 (lane 4 of Figure S3A), and P1-stcDNA-2-FAM/SWNTs + thrombin (lane 5 of Figure S3A), while a clear band of P1 can be observed for the supernatants of P1-stcDNA-2-FAM/SWNTs + T1 (lane 4 of Figure S3B) and P1-stcDNA-2-FAM/SWNTs + thrombin (lane 5 of Figure S3B) if the gel is stained by SYBR Gold. All these results indicate that the formed DNA duplex or DNA (aptamer)−protein complex fell off the SWNT surface and the displaced scDNA resulting from the formation of the more stable dsDNA or DNA−protein complex is directly bound to the SWNT surface; therefore, assembly of scDNA on the SWNT surface is necessary for increasing the fluorescence restoration efficiency.

3.2. Hybridization Kinetics and in Vitro Detection of DNA and Protein. We next investigated whether scDNA can increase the association rate and the fluorescence restoration efficiency. The fluorescence restoration efficiency and the rate of target conjugation to the DNA/SWNT nanocomplex were measured with a P3/SWNT nanocomplex or with a P3-scDNA/SWNT nanocomplex in the presence of one of three unlabeled scDNAs, two short terminal complementary DNAs (stcDNA-1, which is hybridized with the unlabeled terminal region of P3, and stcDNA-2, which is hybridized with the dye-labeled terminal region of P3) and short middle complementary DNA (smcDNA, which is hybridized with the middle region of P3). As expected, all the unlabeled complements can similarly increase the observed rate of target binding and the efficiency of fluorescence restoration (for stcDNA-1, stcDNA-2, and smcDNA, k_{obsd} is 0.095, 0.109, and 0.099 min^{-1} and F_R/F_0 is ca. 36%, 45%, and 40%, respectively) in comparison with the

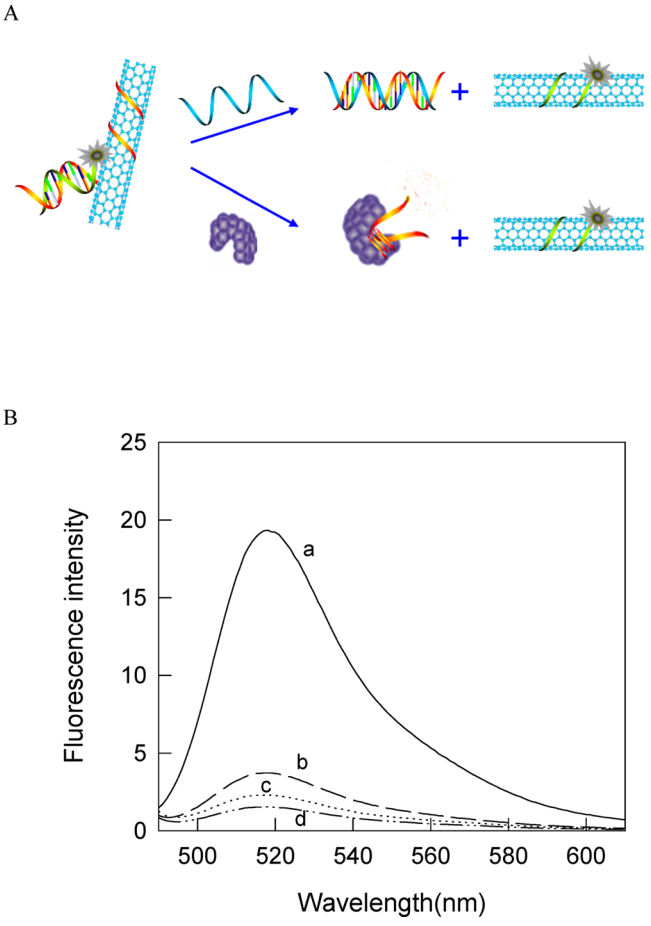

Figure 3. (A) Schematic illustration of the function of scDNA in the DNA/SWNT-based sensing ensemble. (B) Fluorescence emission spectra of the P1-stcDNA-2-FAM/SWNT system with or without targets: (a) P1-stcDNA-2-FAM; (b) P1-stcDNA-2-FAM/SWNTs; (c) P1-stcDNA-2-FAM/SWNTs + T1; (d) P1-stcDNA-2-FAM/SWNTs + thrombin. FAM was excited at λ_{ex} = 480 nm, and both excitation and emission slits are 5 nm.

P3/SWNT nanocomplex (k_{obsd} is 0.044 min^{-1}, and the fluorescence restoration is ca. 12%) (Figure 4). The slight difference in restored fluorescent intensities and kinetic constants depending on the scDNA position might result from the different sequences of the scDNA and the different background fluorescences. These results demonstrated the hypothesis that the scDNA can weaken the affinity of the DNA probe for the SWNT surface by the formation of a dsDNA domain and inhibit the adsorption of the DNA probe–target complexes on the SWNT surface by the competitive assembly of scDNA, thereby resulting in an increase of the response kinetics and fluorescence restoration efficiency. One can also find from Figure 4 that the background fluorescence of the sensing platforms increased with movement of the hybridization site of scDNA toward the dye-labeled terminus. The reason for this phenomenon is that the fluorescence molecule was moved away from the SWNT surface due to the formation of a double-stranded structure.

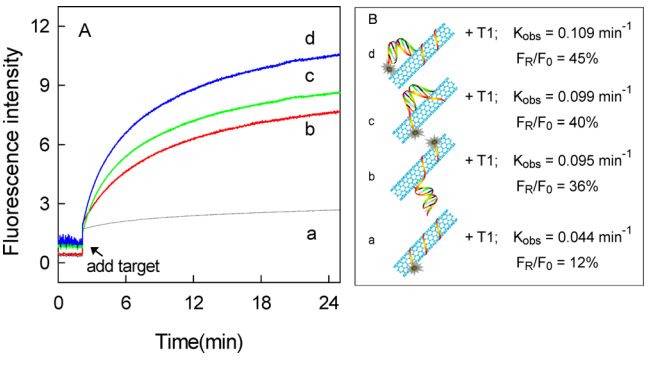

Figure 4. (A) Intensity record of the fluorescence emission at 520 nm when the DNA/SWNT conjugates were incubated with target DNA and (B) schemes of the different DNA/SWNT conjugates and the corresponding binding rates and fluorescence restoration efficiencies calculated from the data shown in (A): (a) P3/SWNTs + T1; (b) P3-stcDNA-1/SWNTs + T1; (c) P3-smcDNA/SWNTs + T1; (d) P3-stcDNA-2/SWNTs + T1. Here, F_0 is 22.53 for 50 nM P3. The experiments were carried out as described in the Experimental Section.

Additionally, the linear detection range and the detection limit were also measured with a P3/SWNT nanocomplex or with a P3-stcDNA-1/SWNT nanocomplex. One can see from Figure 5 that the linear detection range and the detection limit in the presence of scDNA were greatly improved in comparison with those of P3/SWNTs for both DNA target and protein target, which further indicates that the performance of DNA/SWNT-nanocomplex-based biosensing platforms can indeed be improved by the introduction of scDNA.

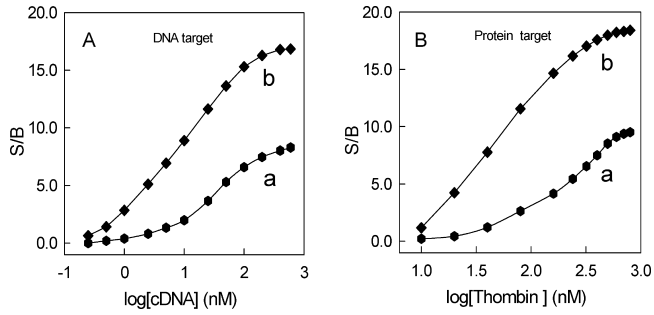

Figure 5. Application of the proposed DNA/SWNT sensing ensemble in the detection of target DNA (A; the concentration of T1 was 0.25, 0.5, 1.0, 2.5, 5.0, 10, 25, 50, 100, 200, 400, and 600 nM, respectively) and protein (B; the concentration of thrombin was 10, 20, 40, 80, 160, 240, 320, 400, 500, 600, 700, and 800 nM, respectively). For curve a, P3/SWNT conjugates were used. For curve b, P3-stcDNA-1/SWNT conjugates were used. The experiments were carried out as described in the Experimental Section.

3.3. Live Cell Imaging. Although carbon nanomaterials, for example, SWNTs, have been proven not only to have the advantage of excellent quenching ability of fluorescence dyes but also to be perfect delivery vehicles to enter cells and single-entity regulation and transfection agents that undergo facile cellular internalization and resistance to enzymatic degradation,[5,22−29] only a few reports can be found that the intracellular detection in the past few decades might be due to the unsatisfactory signaling ability of the ssDNA/SWNTs in living cells. Thus, having established the improved performance of DNA/SWNT sensing platforms with synthetic targets, their ability to detect RNA targets in living cells was further investigated (Figure 6). The DNA probe was designed to incorporate a complementary region for one of the microRNAs (miR21, 5′-UAGCUUAUCAGACUGAUGUUGA-3′). MicroRNAs, which are one subgroup of the small RNA family, have come under intense investigation for their possible applications

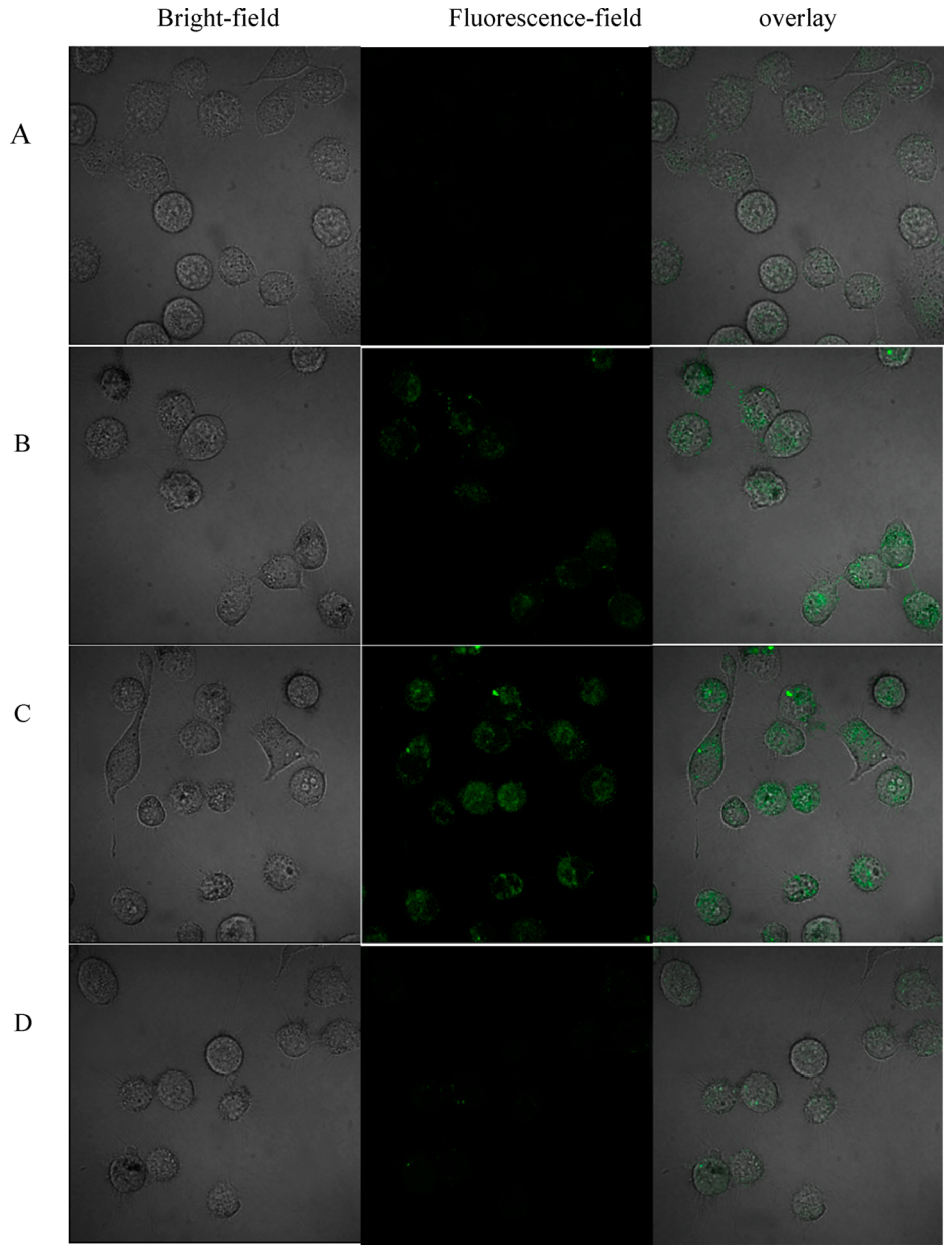

Figure 6. Confocal fluorescence microscopy images of MCF-7 cells after incubation with (A) nothing, (B) P4/SWNTs, (C) P4-scDNA-miR21/SWNTs, and (D) P3-stcDNA-1/SWNTs. The experiments were carried out as described in the Experimental Section.

in cancer detection and typing. These short noncoding RNA molecules act as potent, highly specific regulators of gene expression[30−32] and play roles in cell fate commitment and cell proliferation.[31] Because abnormal cell proliferation is a hallmark of human cancers, researchers believe microRNA expression patterns could denote the malignant state.[33−36] Here, the MCF-7 cell line (human breast cancer), which expresses a high number of miR21's,[37] was used as a model to test miRNA-targeting DNA/SWNT nanoprobes. As a control, P3 with the sequence noncomplementary to the miRNA target was also used for MCF-7 cell imaging in the presence of stcDNA-1. Cells were cultured on glass microscope coverslips, incubated respectively with P3-stcDNA-1/SWNTs, P4/SWNTs, or P4-scDNA-miR21/SWNTs, and imaged using scanning confocal microscopy. MCF-7 cells treated with the P4-scDNA-miR21/SWNT nanoprobes had highly improved fluorescence as compared to those treated with the P4/SWNT nanoprobes, and no significant fluorescence was observed for those treated with the noncomplementary probe P3-stcDNA-1/SWNTs. To further verify the internalization of DNA/SWNT conjugates in MCF-7 cells, *z*-scanning confocal imaging was performed (Figure S4, Supporting Information). It was clear that bright fluorescence was present throughout the whole cells, which suggested efficient delivery of the DNA/SWNT conjugates to the cytosol. These confocal imaging experiments are in excellent agreement with extracellular detection and further demonstrate that improving the performance of carbon nanomaterial/DNA-based sensing platforms by introduction of scDNA is a general strategy that is applicable to a wide range of target detection designs.

4. CONCLUSION

In summary, we have demonstrated that the introduction of certain scDNA sequences can induce changes in the DNA

surface structure that result in a decrease of DNA affinity for SWNTs and move the formed dsDNA domain away from the surface, which can easily initiate target binding, thereby increasing the target association kinetics. Moreover, by competitive assembly of the released scDNA on the SWNT surface, fluorescence restoration can be increased significantly. scDNA increased the response kinetics and fluorescent signal restoration for all of the nucleic acids and surfaces tested, for example, DNA/SWNTs, which can be successfully used for intracellular experiments such as microRNA detection with improved ability. This work represents a significant step forward in the further understanding of association kinetics on surfaces and will be important in a wide range of fields, including bioinformatics, diagnostics, and therapeutics.

■ ASSOCIATED CONTENT

Supporting Information

Electrophoretic analysis of the reaction process, effect of scDNA sequences with different lengths on the sensing platform, gel images for demonstration of the reaction process shown in Figure 3A, and *z*-scanning confocal fluorescence microscopy images of MCF-7 cells incubated with the noted conjugates. This material is available free of charge via the Internet at http://pubs.acs.org.

■ AUTHOR INFORMATION

Corresponding Authors

*E-mail: jishanli@hnu.edu.cn. Fax: +86-731-8882 2523.
*E-mail: yangrh@hnu.edu.cn.

Notes

The authors declare no competing financial interest.

■ ACKNOWLEDGMENTS

This work was supported by the National Natural Science Foundation of China (NSFC) (Grants 21135001, 21205143, and 21305036), the Program for New Century Excellent Talents in University (Grant NCET-13-0188), and the 973 National Key Basic Research Program (Grant 2011CB91100-0).

■ REFERENCES

(1) Zheng, M.; Jagota, A.; Semke, E. D.; Diner, B. A.; McLean, R. S.; Lustig, S. R.; Richardson, R. E.; Tassi, N. G. DNA-Assisted Dispersion and Separation of Carbon Nanotubes. *Nat. Mater.* **2003**, *2*, 338−342.
(2) Wang, S.; Humphreys, E. S.; Chung, S. Y.; Delduco, D. F.; Lustig, S. R.; Wang, H.; Parker, K. N.; Rizzo, N. W.; Subramoney, S.; Chiang, Y. M.; Jagota, A. Peptides with Selective Affinity for Carbon Nanotubes. *Nat. Mater.* **2003**, *2*, 196−200.
(3) Tang, X. W.; Bansaruntip, S.; Nakayama, N.; Yenilmez, E.; Chang, Y. I.; Wang, Q. Carbon Nanotube DNA Sensor and Sensing Mechanism. *Nano Lett.* **2006**, *6*, 1632−1636.
(4) Britz, D. A.; Khlobystov, A. N. Noncovalent Interactions of Molecules with Single Walled Carbon Nanotubes. *Chem. Soc. Rev.* **2006**, *35*, 637−659.
(5) Lu, Q.; Freedman, K. O.; Rao, R.; Huang, G.; Lee, J.; Larcom, L. L.; Rao, A. M.; Ke, P. C. Diffusion of Carbon Nanotubes with Single-Molecule Fluorescence Microscopy. *J. Appl. Phys.* **2004**, *96*, 6772−6675.
(6) Jeng, E. S.; Moll, A. E.; Roy, A. C.; Gastala, J. B.; Strano, M. S. Detection of DNA Hybridization Using the Near-Infrared Band-Gap Fluorescence of Single-Walled Carbon Nanotubes. *Nano Lett.* **2006**, *6*, 371−375.
(7) Kam, N. W.; O'Connell, M.; Wisdom, J. A.; Dai, H. Carbon Nanotubes as Multifunctional Biological Transporters and Near-Infrared Agents for Selective Cancer Cell Destruction. *Proc. Natl. Acad. Sci. U.S.A.* **2005**, *102*, 11600−11605.
(8) Lin, S.; Keskar, G.; Wu, Y.; Wang, X.; Mount, A. S.; Klaine, S. J.; Moore, J. M.; Rao, A. M.; Ke, P. C. Detection of Phospholipid-Carbon Nanotube Translocation Using Fluorescence Energy Transfer. *Appl. Phys. Lett.* **2006**, *89*, 143118.
(9) Wu, W.; Wieckowski, S.; Pastorin, G.; Benincasa, M.; Klumpp, C.; Briand, J. P.; Gennaro, R.; Prato, M.; Bianco, A. Targeted Delivery of Amphotericin B to Cells by Using Functionalized Carbon Nanotubes. *Angew. Chem., Int. Ed.* **2005**, *44*, 6358−6362.
(10) Li, J.; Ng, H. T.; Cassell, A.; Fan, W.; Chen, H.; Ye, Q.; Koehne, J.; Han, J.; Meyyappan, M. Carbon Nanotube Nanoelectrode Array for Ultrasensitive DNA Detection. *Nano Lett.* **2003**, *3*, 597−602.
(11) So, H. M.; Won, K.; Kim, Y. H.; Kim, B. K.; Ryu, B. H.; Na, P. S.; Kim, H.; Lee, J. O. Single-Walled Carbon Nanotube Biosensors Using Aptamers as Molecular Recognition Elements. *J. Am. Chem. Soc.* **2005**, *127*, 11906−11907.
(12) Staii, C., Jr. DNA-Decorated Carbon Nanotubes for Chemical Sensing. *Nano Lett.* **2005**, *5*, 1774−1778.
(13) Hahm, J.; Lieber, C. Direct Ultrasensitive Electrical Detection of DNA and DNA Sequence Variations Using Nanowire Nanosensors. *Nano Lett.* **2004**, *4*, 51−54.
(14) Star, A.; Tu, E.; Niemann, J.; Gabriel, J. C.; Joiner, C. S.; Valcke, C. Label-Free Detection of DNA Hybridization Using Carbon Nanotube Network Field-Effect Transistors. *Proc. Natl. Acad. Sci. U.S.A.* **2006**, *103*, 921−926.
(15) Wang, J.; Liu, G.; Jan, M. R. Ultrasensitive Electrical Biosensing of Proteins and DNA: Carbon-Nanotube Derived Amplification of the Recognition and Transduction Events. *J. Am. Chem. Soc.* **2004**, *126*, 3010−3011.
(16) Yang, R. H.; Tang, Z. W.; Yan, J. L.; Kang, H. Z.; Kim, Y.; Zhu, Z.; Tan, W. H. Noncovalent Assembly of Carbon Nanotubes and Single-Stranded DNA: An Effective Sensing Platform for Probing Biomolecular Interactions. *Anal. Chem.* **2008**, *80*, 7408−7413.
(17) Zhu, Z.; Tang, Z. W.; Phillips, J. A.; Yang, R. H.; Wang, H.; Tan, W. H. Regulation of Singlet Oxygen Generation Using Single-Walled Carbon Nanotubes. *J. Am. Chem. Soc.* **2008**, *130*, 10856−10857.
(18) Welsher, K.; Liu, Z.; Daranciang, D.; Dai, H. J. Selective Probing and Imaging of Cells with Single Walled Carbon Nanotubes as Near-Infrared Fluorescent Molecules. *Nano Lett.* **2008**, *8*, 586−590.
(19) Franchini, M.; Veneri, D. Recent Advances in Hereditary Hemochromatosis. *Ann. Hematol.* **2005**, *84*, 347−352.
(20) Yang, R. H.; Jin, J. Y.; Chen, Y.; Shao, N.; Kang, H. Z.; Xiao, Z. Y.; Tang, Z. W.; Wu, Y. R.; Zhu, Z.; Tan, W. H. Carbon Nanotube-Quenched Fluorescent Oligonucleotides: Probes that Fluoresce upon Hybridization. *J. Am. Chem. Soc.* **2008**, *130*, 8351−8358.
(21) Prigodich, A. E.; Lee, O. S.; Daniel, W. L.; Seferos, D. S.; Schatz, G. C.; Mirkin, C. A. Tailoring DNA Structure To Increase Target Hybridization Kinetics on Surfaces. *J. Am. Chem. Soc.* **2010**, *132*, 10638−10641.
(22) Liu, Z.; Robinson, J. T.; Sun, X. M.; Dai, H. J. PEGylated Nanographene Oxide for Delivery of Water-Insoluble Cancer Drugs. *J. Am. Chem. Soc.* **2008**, *130*, 10876−10877.
(23) Sun, X.; Liu, Z.; Welsher, K.; Robinson, J. T.; Goodwin, A.; Zaric, S.; Dai, H. Nano-Graphene Oxide for Cellular Imaging and Drug Delivery. *Nano Res.* **2008**, *1*, 203−212.
(24) Balapanuru, J.; Yang, J. X.; Xiao, S.; Bao, Q. L.; Jahan, M.; Polavarapu, L.; Wei, J.; Xu, Q. H.; Loh, K. P. A Graphene Oxide−Organic Dye Ionic Complex with DNA-Sensing and Optical-Limiting Properties. *Angew. Chem., Int. Ed.* **2010**, *49*, 6549−6553.
(25) Lu, C. H.; Yang, H. H.; Zhu, C. L.; Chen, X.; Chen, G. N. A Graphene Platform for Sensing Biomolecules. *Angew. Chem., Int. Ed.* **2009**, *48*, 4785−4787.
(26) Jang, H.; Kim, Y. K.; Kwon, H. M.; Yeo, W. S.; Kim, D. E.; Min, D. H. A Graphene-Based Platform for the Assay of Duplex-DNA Unwinding by Helicase. *Angew. Chem., Int. Ed.* **2010**, *49*, 5703−5707.
(27) Jung, J. H.; Cheon, D. S.; Liu, F.; Lee, K. B.; Seo, T. S. A Graphene Oxide Based Immuno-Biosensor for Pathogen Detection. *Angew. Chem., Int. Ed.* **2010**, *49*, 5708−5711.

(28) Wang, X. H.; Wang, C. Y.; Qu, K. G.; Song, Y. J.; Ren, J. S.; Miyoshi, D.; Sugimoto, N.; Qu, X. G. Ultrasensitive and Selective Detection of a Prognostic Indicator in Early-Stage Cancer Using Graphene Oxide and Carbon Nanotubes. *Adv. Funct. Mater.* **2010**, *20*, 3967−3971.
(29) Geim, A. K. Graphene: Status and Prospects. *Science* **2009**, *324*, 1530−1534.
(30) Buchan, J. R.; Parker, R. The Two Faces of miRNA. *Science* **2007**, *318*, 1877−1878.
(31) Hagen, J. W.; Lai, E. C. MicroRNA Control of Cell-Cell Signaling during Development and Disease. *Cell Cycle* **2008**, *7*, 2327−2332.
(32) Kato, M.; Slack, F. J. MicroRNAs: Small Molecules with Big Roles—*C. elegans* to Human Cancer. *Biol. Cell* **2008**, *100*, 71−81.
(33) Calin, G. A.; Croce, C. M. MicroRNA Signatures in Human Cancers. *Nat. Rev. Cancer* **2006**, *6*, 857−866.
(34) Cummins, J. M.; Velculescu, V. E. Implications of Micro-RNA Profiling for Cancer Diagnosis. *Oncogene* **2006**, *25*, 6220−6227.
(35) Tricoli, J. V.; Jacobson, J. W. MicroRNA: Potential for Cancer Detection, Diagnosis, and Prognosis. *Cancer Res.* **2007**, *67*, 4553−4555.
(36) Waldman, S. A.; Terzic, A. MicroRNA Signatures as Diagnostic and Therapeutic Targets. Clinical Chemistry. *Clin. Chem.* **2008**, *54*, 943−944.
(37) Li, J. S.; Schachermeyer, S.; Wang, Y.; Yin, Y. D.; Zhong, W. W. Detection of MicroRNA by Fluorescence Amplification Based on Cation-Exchange in Nanocrystals. *Anal. Chem.* **2009**, *81*, 9723−9729.